ORNL/CP-95522

CONF-971103--

J* Optimization of Small Aspect Ratio Stellarator/Tokamak Hybrid Devices

D. A. Spong, S. P. Hirshman, J. C. Whitson, D.B. Batchelor, B.A. Carreras, V.E. Lynch, and J.A. Rome.
Oak Ridge National Laboratory, Oak Ridge, TN 37830

Abstract

A new class of low aspect ratio toroidal hybrid stellarators is found using a more general plasma confinement optimization criterion than quasi-symmetrization. The plasma current profile and shape of the outer magnetic flux surface are used as control variables to achieve near constancy of the longitudinal invariant J* on internal flux surfaces (quasi-omnigeneity), in addition to a number of other desirable physics target properties. We find that a range of compact (small aspect ratio A), high β (ratio of thermal energy to magnetic field energy), low plasma current devices exist which have significantly improved confinement both for thermal as well as energetic (collisionless) particle components. With reasonable increases in magnetic field and geometric size, such devices can also be scaled to confine 3.5 MeV alpha particle orbits.

I. Introduction

The three-dimensional nature of stellarator configurations offers a vast parameter space of possible design choices for plasma confinement systems. Attractive devices can now be identified out of this space due to the existence of efficient stellarator equilibrium algorithms[1] and multi-dimensional nonlinear optimization techniques[2] coupled with the development of relevant, but easily evaluated, physics target criteria. With respect to plasma transport, an essential advance[3] was the recognition that confinement depended only on the form of |B| in a particular choice of magnetic coordinate system. Although the structure of |B| in these coordinates is directly controlled by the shape of the outer magnetic flux surface, the symmetry properties of |B| in these coordinates can differ from those symmetries (or lack thereof) of |B| and the outer flux surface shape in real space. This fact has allowed significant advances in the confinement quality of stellarator designs and, by allowing adequate confinement of DT fusion produced alpha particles, made them credible as fusion power systems. However, most of these designs have remained at relatively high aspect ratios ($R_0/a > 7$); the reactor embodiment of these devices then necessarily leads to large and expensive systems.

Low aspect ratio, modular-coil stellarator[4,5,6,7,8] designs have recently been developed which offer the attractive features of compact steady-state fusion power systems, high volume utilization, axisymmetric diverted regions, and absence of low order resonances (leading to islands) near the plasma edge. However, studies of confinement in these devices[6] have indicated a need for transport optimization. Of the two quasi-symmetry approaches, only quasi-toroidal optimizations have successfully been achieved[9] at low aspect ratio. The quasi-helical approach[10] is expected to only be applicable at higher aspect ratios.[11] However, in parallel with the quasi-symmetry approaches, various techniques for more directly targeting the drift of particle orbits away from magnetic flux surfaces have also been developed. An initial approach[12,13] in this direction was to focus specifically on improving the confinement of deeply trapped particles, since their orbits can simply be related to contours of the minimum of |B| along the toroidal direction. We have developed a more general method which uses the alignment of the approximate second adiabatic invariant[14,15] J* contours with magnetic flux surfaces. This allows confinement improvement over the entire trapped particle population as well as reduction in the number of transitional particles. Such an approach is equivalent to bounce-averaged omnigeneity, which has recently been interpreted[16,17,18] in terms of equal spacing of |B| contours on a

DISCLAIMER

magnetic flux surface. It has been demonstrated that this equal spacing of |B| is both a necessary and sufficient condition for omnigeneity[17] and that although quasi-helical configurations are omnigenous, the class of nearly omnigenous configurations is much broader than that of quasi-helical systems.[17] Besides allowing confinement improvement at low aspect ratio,[19] this additional flexibility may be expected to better allow for the simultaneous optimization with respect to stability, bootstrap currents, and other physics criteria. In the following we present an example of using the concept of bounce-averaged omnigeneity to generate an actual low aspect ratio stellarator configuration. Our new optimization procedure is first described, followed by an analysis of both the thermal and energetic particle transport properties of the optimized configuration. We find that sizable reductions (factors of $\approx$ 10-20) in thermal particle transport rates can be achieved along with a closing off of the loss cone for more energetic particles. Examination of the |B| spectrum indicates that the optimized state is neither purely quasi-helical nor quasi-toroidal.

II. Description of the Optimization Procedure

Our approach uses the VMEC 3D MHD equilibrium solver[1] augmented with a transformation to Boozer coordinates,[3] as the inner physics evaluation loop of a Levenberg-Marquardt optimization algorithm. The control variables are the shape of the outermost magnetic flux surface, which is expressed in terms of about 20 Fourier harmonics of both R and z, and the plasma current profile. We have applied this optimization technique both to pure currentless stellarators as well as to hybrid systems, but find that the presence of plasma current offers greater flexibility and is generally necessary to attain high β free boundary equilibria. Typically, the optimization targets used are the following: alignment of B_{min}, B_{max}, and J* with magnetic flux contours; matching of $i(\psi)$ to a specified rotational transform profile; maintenance of a magnetic well over most of the plasma cross-section; $R_0/a \approx 3$; avoidance of strongly curved segments on the flux surface; and minimization of magnetic ripple. These target criteria are summarized in Table 1.

Physics goal	Typical target criterion
$B_{extrema}$ and drift and surfaces are aligned with flux surfaces (quasi-omnigeneity). For J* this is done for several values of ε/μ ranging from deeply trapped to nearly passing.	$B_{min} = B_{min}(\psi)$ $B_{max} = B_{max}(\psi)$ $J^* = J^*(\psi)$
Maintain fixed iota	e.g., $i(\psi) = 0.3 - 0.2(\psi/\psi_{max})$
Maintain Magnetic Well	$V'' < 0$
Target low aspect ratio	$R_0/a \approx 3$
Minimize magnetic ripple	Minimize $(B_{max} - B_{min})$
Limit maximum plasma current	$\int_0^r r' dr' j_{plasma}(r') < I_{max}$
Limit local magnetic surface curvature	avoid strong elongation/cusps

Table 1 - Components of stellarator optimization target χ^2 function.

Here B_{min} and B_{max} are the 2D functions of ψ and θ (i.e., magnetic flux and poloidal angle in Boozer coordinates) which are formed by recording the minimum/maximum value of |B| along the toroidal direction within a single field period at fixed ψ, θ. The longitudinal invariant J* is defined as follows:[14,15]

$$J^*(\psi,\theta) = \int_{\psi,\theta=\text{constant}} \frac{g(\psi)d\phi}{B} m|v_{\parallel}| - \sigma_{\parallel}\frac{2\pi}{N}\psi_p$$

$$\text{with } \sigma_{\parallel} = \begin{cases} +1 & \text{co-passing orbits} \\ 0 & \text{locally trapped orbits } (v_{\parallel}=0 \text{ on orbit}) \\ -1 & \text{counter-passing orbits} \end{cases}$$

$$\text{where } v_{\parallel} = \pm\left[\frac{2}{m}(\varepsilon - \mu B - q\Phi)\right]^{1/2}, \; g(\psi) = \text{poloidal current},$$

ψ_p = poloidal magnetic flux function, N = number of field periods,
ε = total energy, μ = magnetic moment, q = charge, m = mass

In general J* contours depend on ψ, θ, ε, ε/μ, and the electrostatic potential Φ. However, for our optimization approach, we shall only target trapped particles and the case where $\Phi = 0$. In this limit, J* only depends on ψ, θ, and ε/μ. For the examples given here, the alignment of the B_{min}, B_{max}, and trapped J* contours with ψ is typically carried out over three or more flux surfaces and, additionally in the case of J*, at four values of the pitch angle variable ε/μ (on a given flux surface, the trapped range of ε/μ is determined by $B_{min,gl} < \varepsilon/\mu < B_{max,gl}$ where $B_{min,gl}$ and $B_{max,gl}$ are the global minima and maxima of B_{min} and B_{max} over the surface). Since the trapped branch of J* is only defined over limited regions of each flux surface [i.e., running from θ_{min} (the trapped/passing boundary at which $\varepsilon/\mu = B_{max}$) to θ_{max} (the trapped/forbidden boundary at which $\varepsilon/\mu = B_{min}$)], its variation is only targeted within these boundaries. χ^2 includes components both to remove the short scale length variations of B_{min}, B_{max}, and J* as well as the longer scale length variations in these quantities over each surface. Each of the target functions is multiplied by an associated weight and summed to form a single χ^2 functional which is to be minimized. The initial condition on the outer flux surface shape is either derived from a free-boundary VMEC equilibrium based on a known set of coils or from a previously optimized configuration.

Once a satisfactorily optimized outer flux surface is found, a second optimization procedure has been developed[20] that varies a parameterized set of coils in order to match $\vec{B}$ at the outer flux surface. In general, this is not a unique process[21] and multiple solutions are possible, depending on the number of coils per field period, the winding surface, etc. By separating the physics and coil optimizations into separate steps, efficiency is gained and a better understanding of the trade-offs of each phase of the design process is possible. In the following, we will discuss only the physics (i.e., outer flux surface) optimization.

III. Example of an Optimized Configuration

This optimization technique has been applied to an 8 field period, hybrid stellarator/tokamak device with major radius R_0 = 1.3m, B_{axis} = 1.2 Tesla, $R_0/a \approx 2.8$, $\langle\beta\rangle$ = 2%, and a plasma current of around 60 kA. We will compare the initial un-optimized device, whose flux surface shape was determined by a set of 8 external modular coils, with an optimized configuration based on the alignment of J* with ψ. Figure 1 shows 3D rendered flux surfaces for the two configurations with the grayscale shading used to indicate the constant |B| contours. The iota profile in the unoptimized case runs from a maximum of about 0.3 to 0.15 at the edge with a central region of reversed shear while that of the optimized case covers a similar range, but has a reversed shear region near the edge.

The optimized case also has lower levels of ripple near the magnetic axis. In Figures 2(a) and 2(b) the B_{min} contours are shown for the two cases, indicating that the unoptimized configuration (a) has completely unclosed B_{min} contours (i.e., all deeply trapped particles are lost), while the optimized configuration (b) has large regions of closed B_{min} contours. We have also examined the J* contours over a range of pitch angles and find that they are more closely aligned with flux surfaces than in the original configuration.

As mentioned earlier, the J* optimization process leads to configurations which are neither quasi-toroidal nor quasi-helical. This is demonstrated in Figures 3(a) and 3(b) where we have plotted the B_{mn} coefficients at the edge (excluding the m = 0 modes) vs. the resonance frequency n/m - ι for (a) the un-optimized case and (b) the J* optimized case. Although the spread of the higher order modes has been reduced in Figure 3(b), it still contains significant $n \neq 0$ terms and a mixture of different helicities.

The approach to bounce-averaged omnigeneity through the alignment of trapped particle J* surfaces with flux surfaces should be approximately equivalent to the criterion of equal angular separation between constant |B| contours on a flux surface which has been suggested recently in Refs. 16-18. The differences between these criteria are of order ι/N (N = number of field periods) due to the use of the exact J (integral along a field line) and J* (integral along ϕ_{Boozer}) and are generally small for the configurations examined here. We have confirmed this by plotting contours of equal toroidal angle separation between a range of |B| values and find that these contours are very similar to those of the equivalent J* surfaces (i.e., at $\varepsilon/\mu = |B|$).

IV. Confinement Properties of the Optimized Configurations

In conjunction with the above optimization process, it is important to use various measures to evaluate the optimized configurations. As the optimization will not generally lead to precise alignment of J* and magnetic flux surfaces, it is difficult to judge the relative merits of different optimized cases simply by plotting the resulting J* contours. We have chosen to evaluate both the transport of thermal plasma and the confinement of energetic species (e.g., as required for plasma heating). Both of these measures are too time-consuming to be incorporated directly into the optimization loop.

(A) Thermal Transport

In order to compare the thermal transport of the configurations presented in Section II, we have chosen to follow the Monte Carlo evolution[22] of 256 particles started at a single radial location ($\psi = 0.25\psi_{max}$) with a random distribution in pitch angle, poloidal and toroidal angles, and a monoenergetic distribution in energy. The background plasma has a density of 5×10^{13} cm^{-3} and a temperature of 1 keV; the test particle energy is also 1 keV. The ratio of the collision frequency to the bounce frequency is around 10^{-3}, placing the plasma in a regime where large helical ripple losses would occur without optimization. The same random number seed was used for each configuration so that initial conditions are equivalent. We monitor the escape of particles and energy through the outer flux as a function of time and use this as our basic measure of thermal confinement. This loss rate has the advantage of including both the direct prompt orbit losses as well as diffusive losses and involves no assumptions regarding localized transport.

In Figure 4 we show the particle loss rates vs. time for the original, B_{min}-optimized, and J*-optimized cases along with an equivalent tokamak case. The latter configuration is arrived at from the J* optimized case by retaining only the n = 0 harmonics. These results clearly demonstrate that the optimization procedure can substantially reduce loss rates, leading to about a factor of 10 reduction over the initial unoptimized configuration. The J* optimized case is also within a factor of 3-4 of the equivalent tokamak loss rates.

A further interesting consequence of quasi-omnigenous systems is that transport is not automatically ambipolar and they therefore retain some degree of dependence of transport rates on the radial electric field. Quasi-symmetric configurations should be isomorphic to tokamak transport[23] which is independent of the electric field. In Figure 5 we show examples of transport levels for the above J* optimized case in the presence of a potential profile which is zero at r = 0 and rises near the plasma edge. As may be seen, moderate levels of electric field can suppress density losses even below the equivalent tokamak level.

We next vary the background plasma density over the range of 10^{12} cm^{-3} to 10^{14} cm^{-3} to examine the collisionality scaling of transport for the J* optimized configuration (in this case with $e\phi/kT_{ion} = 0$). The results shown below in Figure 6 indicate that transport in the J* optimized configuration has a similar dependence as the tokamak and shows no evidence of a $1/\nu$ ripple transport regime.

(B) Energetic Particle Transport

The confinement of collisionless energetic particles is one of the primary motivations for the optimizations discussed here since the thermal particle confinement can, even without optimization, be improved by control of the ambipolar electric field.[6] Due to the fact that most heating schemes rely on some form of energetic particle tail population, heating efficiencies can depend sensitively on the confinement of this species.

In order to compare the two configurations we have followed orbits at 40 keV which initially pass through the magnetic axis over a range of pitch angles and find that the unoptimized configuration has a loss cone over $-0.2 < (v_{\|}/v)_0 < 0.4$. In contrast, the J* optimized configuration has no loss cone and confines the same orbits over the full range of $(v_{\|}/v)_0$. Besides confining the trapped orbits, the optimization also reduces the deviations of passing orbits away from flux surfaces. The deeply trapped orbits in the optimized configuration move on superbanana trajectories (i.e., banana shaped orbits formed by many longitudinal bounces within a field period) and are confined up to energies at which their drift per bounce becomes too large for the longitudinal invariant J* to be conserved. For the example configuration considered here, this occurs at around 400 keV. In Figures 7(a) and 7(b) we display orbits in the J* optimized configuration with increasing energy for (a) a deeply trapped orbit $[(v_{\|}/v)_0 = 0.1]$ and (b) a co-passing orbit $[(v_{\|}/v)_0 = 1.0]$ for energies of 100, 200, and 400 keV. The trapped orbit has lost confinement at around 400 keV. The passing orbits are still confined, but with significant displacements away from flux surfaces ($\Delta/a \approx 0.5$). The deeply trapped orbits show an interesting property of confined superbanana stellarator orbit trajectories in that, unlike normal tokamak banana orbits, the superbanana width is essentially independent of energy (i.e., due to the fact that for trapped particles and in the absence of electric fields J* does not depend on energy). To the extent that J* is conserved, relatively arbitrary energies will be confined on the same trajectory. The point at which J* conservation is lost due to the drift per bounce becoming too large can be extended by increasing the B field or increasing the device size.

By scaling up the magnetic field and determining the maximum confined energy, we have predicted the increase in geometric size and magnetic field which would be required to confine 3.5 MeV alpha particles in our J* optimized example. In Figure 8 the loss fraction of alphas is plotted as the energy is gradually increased. Here we have again only checked orbits passing through the magnetic axis and have scanned over the full range of pitch angles $-1 < v_{\|0}/v < +1$. At a certain energy, the loss fraction rises steeply. f_B is the scale factor by which the magnetic field is increased. As f_B is increased, orbits can be confined at progressively higher energies. At around f_B = 4-5, it becomes possible to confine a significant fraction ($\approx$ 90%) of 3.5 MeV alphas. This information can then be plotted in terms of the energy at which a specified level of loss occurs vs. the scaling factor, f_B, as shown in Figure 9. Both the drift per bounce (which determines the maximum energy of

confined trapped orbits) as well the ratio of the displacement of passing orbits to the minor radius scales as ρ/a, where ρ is the gyroradius. Figure 9 confirms this scaling (indicated by the straight lines) for both levels of loss up to at least 3.5 MeV. From these results, one could predict, for example, that if both the magnetic field and size were scaled up by a factor of ≈ 2 one begins to confine a significant fraction of alphas.

IV. Conclusions

We have developed a new optimization procedure for low aspect ratio stellarators which targets bounce-averaged omnigeneity (i.e., minimization of drift away from the flux surface) by aligning contours of the approximate second adiabatic invariant J* with magnetic flux surfaces. This technique uses the shape of the outermost flux surface and the plasma current profile as control parameters. Our optimization has led to qualitatively new kinds of stellarator configurations which are neither quasi-toroidal nor quasi-helical. This additional flexibility in the |B| spectrum has opened up the available parameter space at low aspect ratio and resulted in significant improvements in confinement of both thermal as well as energetic particle components. For example, thermal transport can approach that of axisymmetric systems. We also find that with reasonable scaleups in size and magnetic field, it is possible to confine 3.5 MeV alpha orbits. We expect that such flexibility will allow inclusion of further criteria[24] related to MHD ballooning stability as well as other physics issues which may be of importance. Evaluations of ballooning stability in these configurations have already indicated that volume-averaged $<\beta>$'s of 6% are stable. The coil reconstruction for these optimized states is relegated to a separate step and appears feasible, but will require further development.

Acknowledgment

Research sponsored by the Office of Fusion Energy U. S. Department of Energy, under contract DE-AC05-960R22464.

[1] S. P. Hirshman, J. C. Whitson, Phys. Fluids **26** 3553 (1983).
[2] P.E. Gill, W. Murray, and M.H. Wright, *Practical Optimization*, (Academic Press, London, 1981).
[3] A .H. Boozer, Phys. Fluids **23**, 904 (1980).
[4] B. A. Carreras, N. Dominguez, L. Garcia, et al., Nuclear Fusion **28** 1195 (1988).
[5] B. A. Carreras, V. E. Lynch, A. Ware, ORNL/TM-13252, (June, 1996).
[6] D. A. Spong, S. P. Hirshman, J. C. Whitson, Plasma Physics Reports **23** 483 (1997).
[7] P. E. Moroz, Phys. Rev. Lett. **77** 651 (1996).
[8] D. W. Ross, P. M. Valanju, H. He, W. H. Miner, P. E. Phillips, J. C. Wiley, A. J. Wooton, S-B. Zheng, Plasma Physics Reports **23** 492 (1997).
[9] P. R. Garabedian, Phys. Plasmas **3** 2483 (1996).
[10] J. Nührenberg, R. Zille, Phys. Lett. **A129** 113 (1988).
[11] D. A. Garren, A. H. Boozer, Phys. Fluids **B 3** 2822 (1991).
[12] R. N. Morris, C. L. Hedrick, S. P. Hirshman, J. F. Lyon, J. A. Rome, Proc. 7th Int. Workshop on Stellarators, Oak Ridge, TN, April 10-14, 1989, IAEA, Vienna (1989).
[13] S. P. Hirshman, et al., ibid.
[14] J. R. Cary, C. L. Hedrick, J. Tolliver, Phys. Fluids **31** 1586 (1988).
[15] J. A. Rome, Nuclear Fusion **35** 195 (1995).
[16] A. A. Skovoroda, V. D. Shafranov, Plasma Physics Reports, **21** 937 (1995).
[17] J. R. Cary, S. G. Shasharina, Phys. Rev. Lett. **78**, 674 (1997).
[18] H. Weitzner, Phys. of Plasmas, **4**, 575 (1997).
[19] S. P. Hirshman, D. A. Spong, J. C. Whitson, D. B. Batchelor, B. A. Carreras, V. E. Lynch, J. A. Rome, to be published in Phys. Rev. Lett., 1997.

[20] S. P. Hirshman, J. C. Whitson, D. A. Spong, "Modular Coil Design for Optimized Stellarators," in preparation.
[21] P. Merkel, J. Comput. Phys. **66** 83 (1986).
[22] R. H. Fowler, J. A. Rome, J. F. Lyon, Phys. Fluids **28** 338 (1985).
[23] A. H. Boozer, Phys. Fluids **26** 496 (1983).
[24] W. A. Cooper, Phys. Plasmas **4** 153 (1997).

Figures

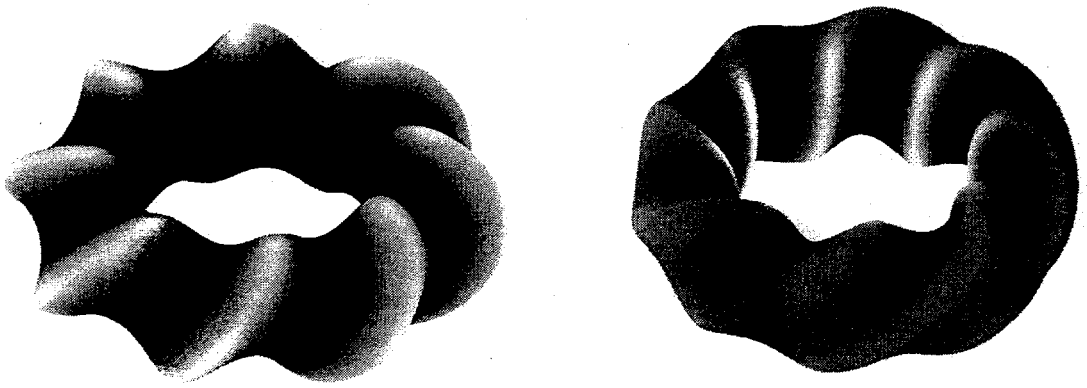

(a) (b)

Figure 1. Outer flux surface shape with grayscale shading proportional to |B| magnitude (darker areas are higher field) for (a) an unoptimized configuration and (b) a J* optimized configuration.

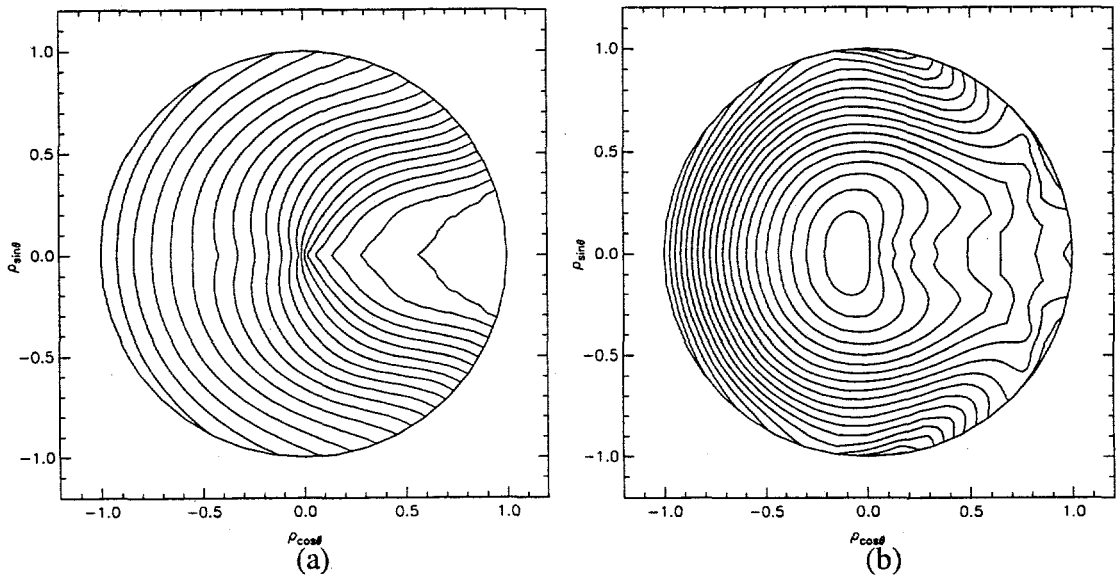

Figure 2. B_{min} contours for (a) unoptimized and (b) J*-optimized configurations.

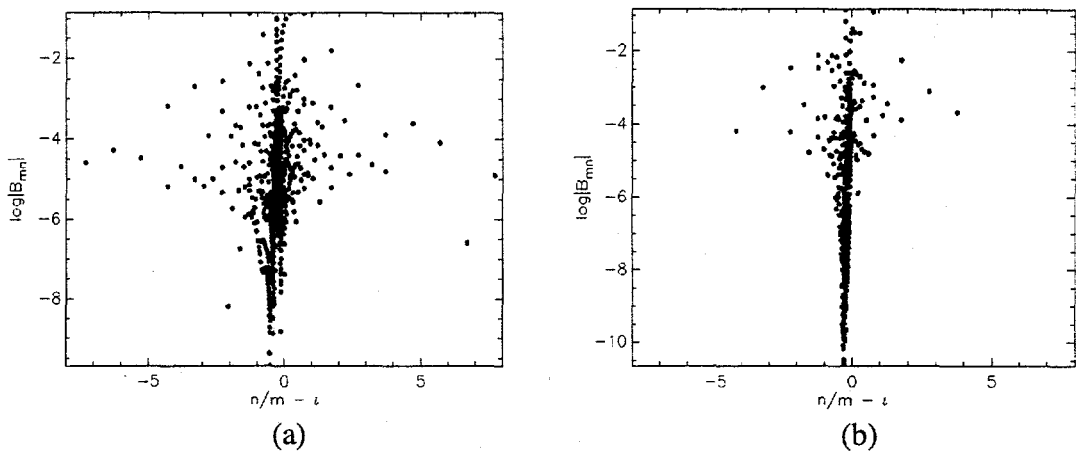

Figure 3. B_{mn} coefficients evaluated at the plasma edge vs. the resonance frequency n/m - i for (a) the unoptimized case and (b) the J*-optimized case.

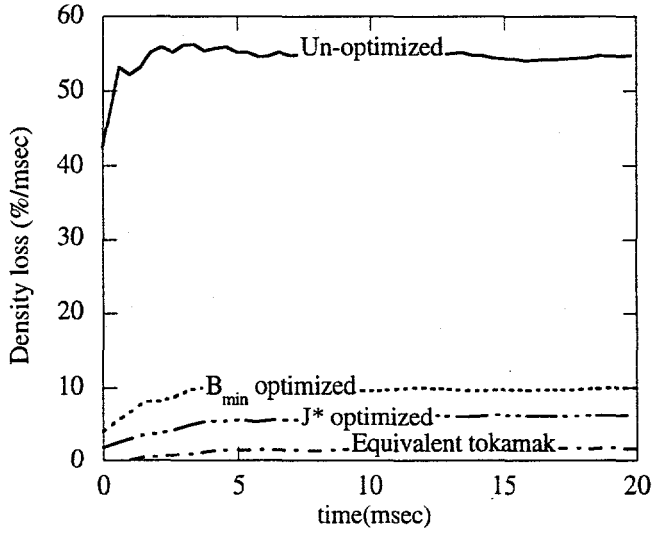

Figure 4. Monte Carlo particle loss rates through the last closed flux surface vs. time for the original unoptimized configuration, a B_{min} optimized configuration, a J* optimized configuration, and an equivalent tokamak.

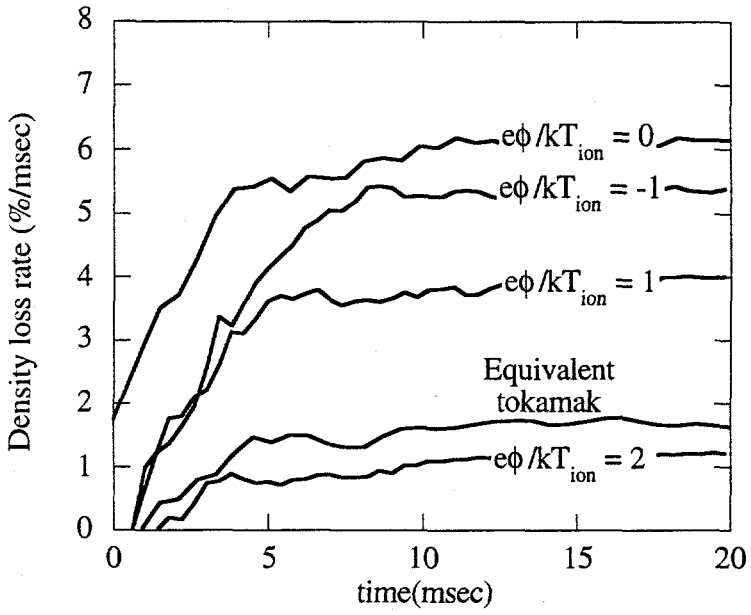

Figure 5. Monte Carlo particle loss rates for the J* optimized case with various levels of radial ambipolar electric field present.

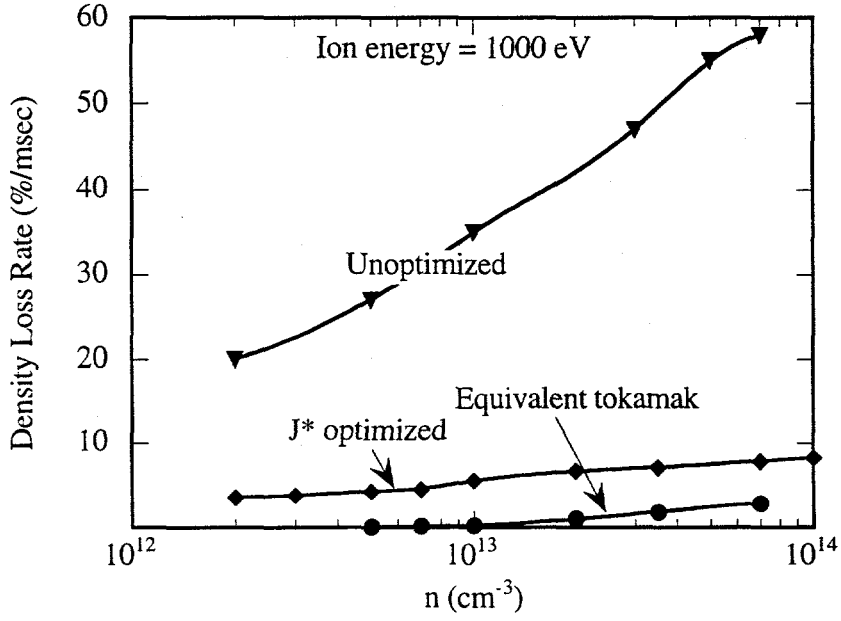

Figure 6. Scaling of loss rates with density (collisionality) for : the original unoptimized case, the J* optimized case (with $e\phi/kT_{ion} = 0$) and equivalent tokamak case.

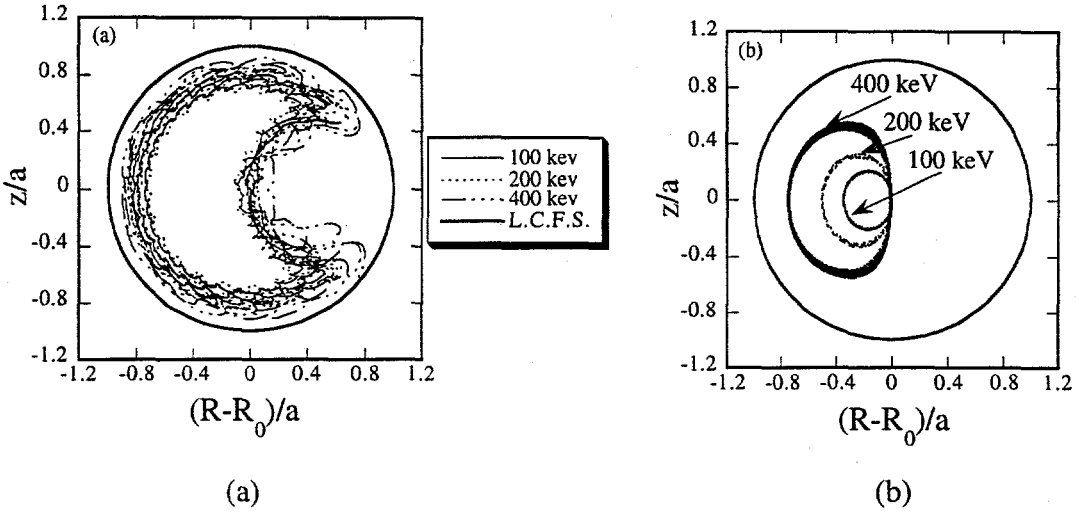

Figure 7. Ion orbits which pass through the magnetic axis at 100 keV, 200 keV, and 400 keV in the J*-optimized case for (a) $v_{||0}/v = 0.1$ (trapped) and (b) $v_{||0}/v = 1.0$ (passing).

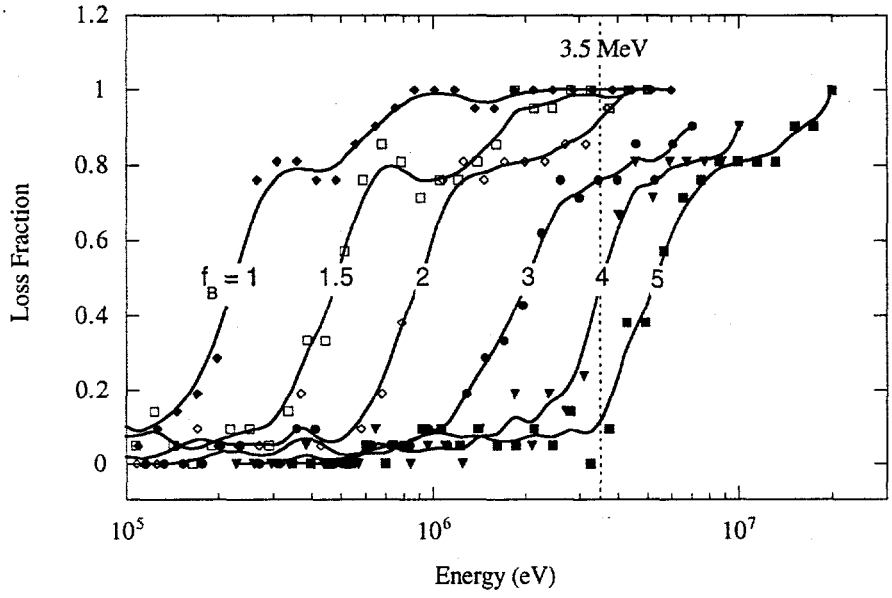

Figure 8. Alpha particle loss fractions vs. energy and scaling factor (f_B) in the product of size and magnetic field.

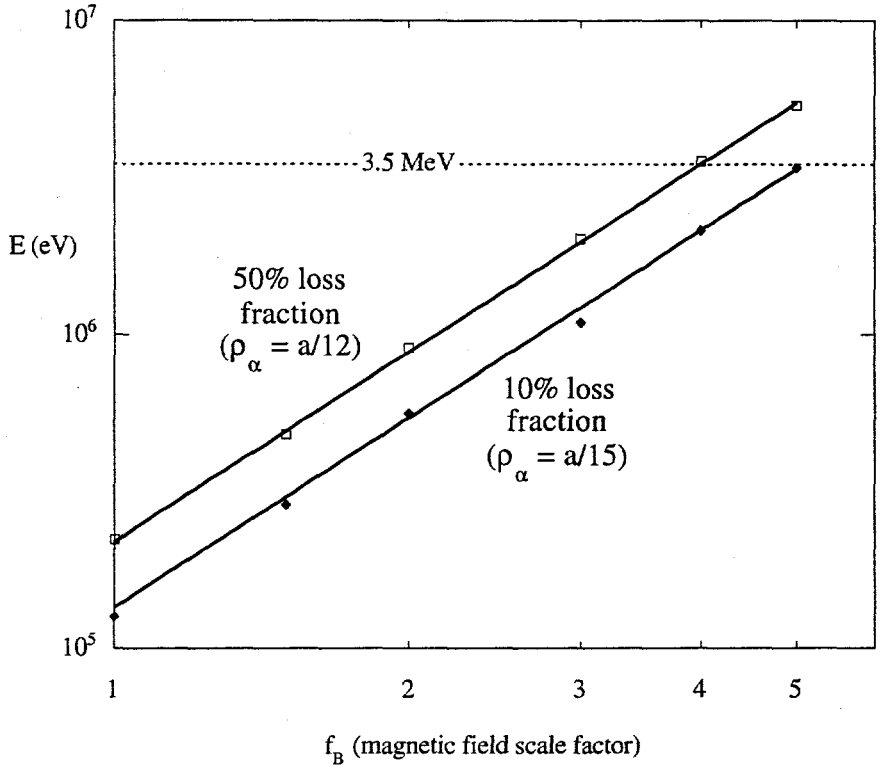

Figure 9. ρ_α/a scaling of various levels of alpha particle loss vs. energy and f_B.